New Folder Name External Phase Modulation

"External Phase Modulation Interferometry," by Malcolm B. Gray, Andrew J. Stevenson, Charles C. Harb, Hans-A. Bachor, David E. McClelland, July 12, 1994

Distributed by S. Whitcomb 7/22/94

PLEASE PASS ALONG PROMPTLY

COPY 1

A. Abramovici
J. Camp
J. Carri
D. Durance
A. Gillespie
S. Kawamura
A. Kuhnert
T. Lyons

COPY 2

J. Mason
R. Savage
V. Schmidt
L. Sievers
R. Spero
M. Zucker

cc: B. Barish
F. J. Raab
M. Regehr
R. Vogt
S. Whitcomb -original
MIT Science Group
Project File
Science File

LIGO

Technical Report 94.1

July 12, 1994

External Phase Modulation Interferometry

Malcolm B Gray, Andrew J Stevenson, Charles C Harb
Hans-A Bachor, David E McClelland

Department of Physics and Theoretical Physics
Faculty of Science
The Australian National University
Canberra ACT 0200
Australia

1. Introduction

In this report, we investigate the performance and operational requirements of a generic external modulation scheme, in which the output of a Michelson interferometer is coherently combined with a reference beam tapped off the input beam. This constitutes a Michelson interferometer within a Mach-Zehnder interferometer.

In Section 2 we analyse our generic model and derive the expected signal-to-noise performance, accounting for non-ideal features one might expect in practice. We find that both electronic noise in the detectors and imperfect fringe contrast in the Michelson interferometer increase the required optical power tap-off fraction, and reduce the achievable sensitivity. By contrast, we find that the optimum phase modulation depth in the local oscillator arm and the required DC optical phase settings for both the Michelson and local oscillator arms are fixed, regardless of interferometric fringe visibility or detection system quality.

We find that the ultimate achievable sensitivity in an ideal external modulation system is comparable with that of internal modulation, and that both schemes (for different reasons) suffer about a 33% sensitivity penalty compared to ideal shot-noise-limited direct detection, when simple modulation and demodulation waveforms are used.

Section 3 describes our optical and electronic configuration, including technical considerations affecting the design, such as the need to achieve reasonable Gaussian beam matching throughout the interferometer, to adjust the optical power tap-off fraction into the local oscillator beam, and to compensate vibrational disturbances in the interferometer with piezo-controlled mirrors. Our

layout is designed to match the theoretical model as far as possible, to confirm the analytic predictions.

Section 4 describes our experiments, performed to measure the achievable interferometric sensitivity, to compare the results to theoretical predictions, and to investigate aspects of the technical design of practical interferometers which do not fall into the realm of an analytic model. Our Michelson interferometer has a high contrast ratio (~ 600:1 in some instances) while the equivalent ratio in the Mach Zehnder is more like 100:1 when optimised. We find when using an input optical power of around 9mW, that electronic noise arising in our detectors and amplifiers is the dominant noise component dictating the optimal power splitting fraction and the ultimate sensitivity. In our measurements, electronic noise is greater by a factor of ~60 than the shot noise associated directly with the dark fringe transmission from the Michelson. This indicates that the Michelson could have a fringe contrast as poor as 10:1, or the laser power could be as high as 500 mW, before the dark fringe shot noise figures as prominently as electronic noise.

The main feature dictating our suppression of laser technical noise is our ability to lock the Michelson interferometer to its dark fringe and reduce the residual RMS phase deviations. By means of an integrating servo loop with a 5 kHz response bandwidth, we are able to suppress acoustic vibrations in the Michelson interferometer sufficiently to eliminate laser intensity noise (including the strong relaxation oscillation peaks) and thus enable shot-noise-limited sensitivity down to ~ 100 kHz, where laser frequency fluctuations remained the dominant noise contribution. These frequency fluctuations couple into the signal intensity spectrum due to the optical path length mismatch inside the Michelson interferometer.

Section 5 highlights our principal findings and conclusions.

2. External modulation interferometry : A generic model

2.1 Motivations for using external modulation

The optical power emerging from a Michelson interferometer fluctuates due to changes in the effective optical path difference between the two interferometer arms, and also due to input intensity fluctuations such as technical noise of the laser source. The desired signal from the interferometer may be completely masked by the technical laser noise, even if the detected optical power is relatively low.

Combining the Michelson output with a coherent phase-modulated beam at a beam combiner, as depicted in Fig. 1, will result in a homodyne photocurrent containing an additional intensity modulation at the applied phase modulation frequency, in general, as well as components at the sum and difference of the modulation and signal frequencies. These sum and difference frequency components will yield the required signal information after demodulation. Technical noise can be

nulled out in the same process by selecting the correct interferometer and local oscillator phases. We now demonstrate analytically how this works.

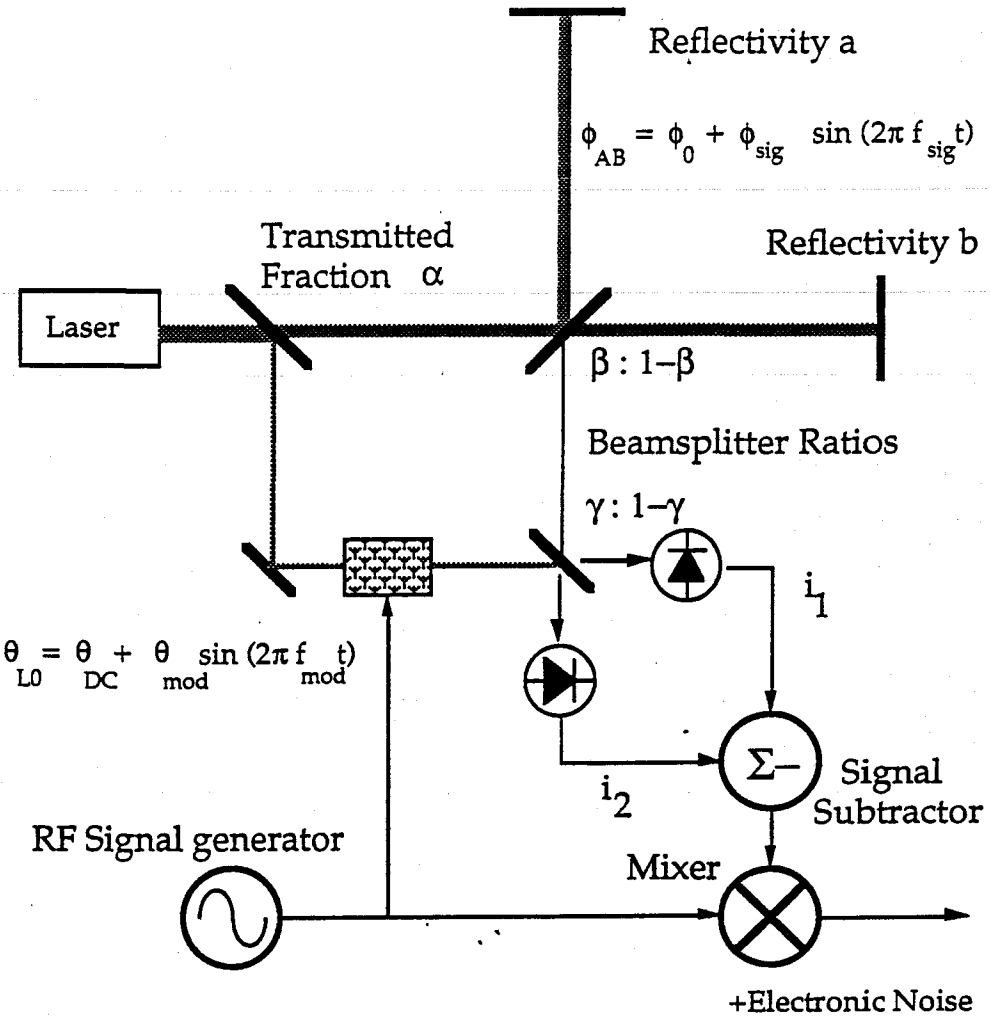

Figure 1: Schematic plan of a generic external modulation interferometer.

2.2 Optical fields in the interferometer

In this analysis, we will assume perfect matching of all beams in the interferometer, ie. all beams have the same wavefront curvature at points of interference, ie. at the detectors, and all transverse field distributions are identical at the photodetectors. We also assume that the entire optical field is detected at each photodetector. In this model, therefore, all fields are parametrised by just two quantities - *Amplitude* and *Phase*.

We model changes in the arm length difference in the interferometer by equal and opposite phase changes in the two arms $\phi(t)/2$. The input light is associated with an electric field amplitude E, and is split into two beams at a simple lossless beamsplitter (loss is modelled by assuming a smaller effective input field E). The interferometer input field has amplitude:

$$E_{mi} = \alpha^{1/2} E \qquad (1)$$

where α is the (power) transmissivity of the tapoff beamsplitter. An ideal passive beamsplitter introduces a relative phase of $\pi/2$ between the two output fields, so we may write the local oscillator field emerging from the beamsplitter in complex notation:

$$E_{lo} = i(1-\alpha)^{1/2}E \tag{2}$$

We now trace both beams through the apparatus to determine what field amplitudes will add at the detectors after the final beam combiner.

The interferometer input field is split at a 50:50 beam-splitter (losses subsumed into the non-ideal, end mirror reflectivities), propagates along each arm of the Michelson to a non-ideal mirror, and back again, recombining at the beamsplitter to produce an output field

$$E_{mo} = i\alpha^{1/2}E\,(e^{i\phi/2}\sqrt{a} + e^{-i\phi/2}\sqrt{b})/2 \tag{3}$$

where a and b are the power reflectivities of the two end mirrors in arm A and arm B respectively. The factor of i signifies the $\pi/2$ phase shift incurred by each component undergoing one transmission and one reflection at the beamsplitter to get from the interferometer input to its output.

The electric fields incident on the two photodetectors are then a coherent sum of the Michelson output field and the modulated local oscillator field, taking into account phase shifts incurred in the local oscillator arm ($\theta = \theta(t)$, due to the combined effects of the external arm phase modulator and the DC optical path difference) and in the final beam combiner ($\pi/2$):

$$\begin{aligned} E_1 &= (E_{mo} + iE_{lo}e^{i\theta})/\sqrt{2} \\ &= (E/\sqrt{2})\left[i\alpha^{1/2}E\,(e^{i\phi/2}\sqrt{a} + e^{-i\phi/2}\sqrt{b})/2 - (1-\alpha)^{1/2}e^{i\theta}\right] \end{aligned} \tag{4a}$$

$$\begin{aligned} E_2 &= (iE_{mo} + E_{lo}e^{i\theta})/\sqrt{2} \\ &= (E/\sqrt{2})\left[-\alpha^{1/2}(e^{i\phi/2}\sqrt{a} + e^{-i\phi/2}\sqrt{b})/2 + i(1-\alpha)^{1/2}e^{i\theta}\right] \end{aligned} \tag{4b}$$

2.3 Photocurrents

These fields produce photocurrents proportional to the square of their magnitude. We *define* the detector responsivity ρ in terms of the induced photocurrent I(t) due to an incident electric field E(t), assuming detector response much faster than the fastest intensity fluctuations:

$$I(t) = \rho\, E(t)\, E^*(t) \tag{5}$$

The photocurrents from the two detectors are then given by substituting (4a) and (4b) into (5):

$$I_1 = (E^2\rho/2)\left\{(a+b)\,\alpha/4 + (1-\alpha) + \cos\phi\ (ab)^{1/2}\alpha/2 - (\alpha(1-\alpha))^{1/2}\left[\sqrt{b}\sin(\phi/2+\theta) - \sqrt{a}\sin(\phi/2-\theta)\right]\right\} \quad (6a)$$

$$I_2 = (E^2\rho/2)\left\{(a+b)\,\alpha/4 + (1-\alpha) + \cos\phi\ (ab)^{1/2}\alpha/2 + (\alpha(1-\alpha))^{1/2}\left[\sqrt{b}\sin(\phi/2+\theta) - \sqrt{a}\sin(\phi/2-\theta)\right]\right\} \quad (6b)$$

The signal phase ϕ and the modulation phase θ are time dependent, and for simplicity, we will assume sinusoidal variations as follows:

$$\phi = \phi_0 + \phi_s \sin(\omega_s t) \quad (7a)$$

$$\theta = \theta_0 + \theta_m \sin(\omega_m t) \quad (7b)$$

Here, ϕ_0 and θ_0 are the DC phase offsets in the Michelson interferometer and the local oscillator beam respectively, while ϕ_s and θ_m are modulation depths due to the signal and external modulation at frequencies ω_s and ω_m respectively.

2.4 Frequency components in the photocurrents

Substituting the phase variations (7a) and (7b) into (6a) and (6b) gives an expression for photocurrent which can be expanded using Bessel functions. The current exhibits DC and AC components, at frequencies corresponding to the baseband modulations at ω_s and ω_m, intermodulation components at $\omega_m \pm \omega_s$, as well as higher order harmonics which will not figure in the demodulation process to follow. We now give expressions for the components of interest.

The DC photocurrent in each detector is as follows:

$$I_{1,2}(DC) = (E^2\rho/2)\left\{(1-\alpha) + \alpha\left[(a+b)/4 + \cos\phi_0\,(ab)^{1/2}J_0(\phi_s)/2\right] \pm (\alpha(1-\alpha))^{1/2}\,J_0(\phi_s/2)\,J_0(\theta_m) \times\left[\sqrt{a}\sin(\phi_0/2-\theta_0) - \sqrt{b}\sin(\phi_0/2+\theta_0)\right]\right\} \quad (8)$$

where the $\pm$ sign refers to current at detectors 1 (+) and 2(-). The first three terms represent the total DC power incident on the two beam combiner ports. The term $(1-\alpha)$ represents power from the local oscillator arm, and the other two terms proportional to α represent power emerging from the Michelson interferometer, complete with the standard phase dependence $\cos\phi_0$. When there is no signal in the interferometer, $J_0(\phi_s)$ becomes unity and perfect fringe contrast can result if a = b (identical mirrors). The presence of signals in the interferometer destroys the perfect interference in this DC picture, because the phase variations allow light to be transmitted through the interferometer even when the DC phase ϕ_0 is set to 0.

The term following the ± sign, proportional to $\sqrt{[\alpha(1-\alpha)]}$, represents power variation at the detectors due to phase differences between the local oscillator and the Michelson output.

Laser intensity noise at low frequencies is carried implicitly in the E^2 factor. (It is this feature which prevents direct detection at the shot noise limit for low frequency signals.)

The baseband signal component (which can be lost in intensity noise associated with the DC component) is:

$$I_{1,2}(\omega_S) = E^2 \rho \left\{ -\alpha \sin\phi_0 (ab)^{1/2} J_1(\phi_s)/2 \pm (\alpha(1-\alpha))^{1/2} J_1(\phi_s/2)\, J_0(\theta_m) \left[\sqrt{a}\cos(\phi_0/2 - \theta_0) - \sqrt{b}\cos(\phi_0/2 + \theta_0)\right]\right\} \times \sin(\omega_S t) \quad (9)$$

where again the ± sign refers to detectors 1 and 2 respectively. The first term represents the square law detector response to optical sidebands and carrier emerging from the Michelson. The term following the ± sign represents interaction between optical sidebands emerging from the Michelson and the optical carrier of the local oscillator.

Similarly, a component appears at the external modulation frequency :

$$I_{1,2}(\omega_m) = \mp E^2 \rho (\alpha(1-\alpha))^{1/2} J_0(\phi_s/2)\, J_1(\theta_m) \times \left[\sqrt{a}\cos(\phi_0/2 - \theta_0) + \sqrt{b}\cos(\phi_0/2 + \theta_0)\right] \sin(\omega_m t) \quad (10)$$

This component is solely due to interaction at the detector between the optical carrier from the Michelson and the external modulation sidebands from the local oscillator. There is no self-interaction between the local oscillator sidebands and its own carrier, as these retain strict phase modulation symmetry. This component, like the DC component in Equation (8) carries its own complement of laser intensity noise showing up as a modulation of the E^2 factor. This can be viewed in the frequency domain as a consequence of the convolution theorem - both signals and noise are shifted to higher frequencies centred around ω_m by a modulation at ω_m.

Finally, the component containing the shifted signal information is given by :

$$I_{1,2}(\omega_m \pm \omega_s) = \pm E^2 \rho(\alpha(1-\alpha))^{1/2} J_1(\phi_s/2)\, J_1(\theta_m) \times \left[\sqrt{a}\sin(\phi_0/2 - \theta_0) + \sqrt{b}\sin((\phi_0/2 + \theta_0)\right] \times \left[\cos(\omega_m - \omega_s)t - \cos(\omega_m + \omega_s)t\right] \quad (11)$$

These shifted components are due to the interaction at the detector between the optical modulation sidebands from the Michelson and Local Oscillator beams.

The photocurrent from detectors 1 and 2 are then combined in a R.F. splitter/combiner. The 180° output of the R.F. splitter/combiner is expressed as:

$$I_{\Sigma-} = (I_1 - I_2)/\sqrt{2} \tag{12}$$

Performing this subtraction operation on the frequency shifted signal sidebands results in:

$$\begin{aligned} I_{\Sigma-}(\omega_m \pm \omega_s) = \; & \sqrt{2}\, E^2 \rho\, (\alpha\,(1-\alpha))^{1/2}\, J_1(\phi_s/2)\, J_1(\theta_m) \\ & \times \left[\sqrt{a}\, \sin(\phi_0/2 - \theta_0) + \sqrt{b}\, \sin((\phi_0/2 + \theta_0)\right] \\ & \times \left[\cos(\omega_m t - \omega_s t) - \cos(\omega_m t + \omega_s t)\right] \end{aligned} \tag{13}$$

2.5 Demodulation of the frequency-shifted signals and noise

The operation of the mixer is to shift this signal back to baseband. This is achieved by multiplying the subtracted photocurrent output by a sinusoid at the modulation frequency:

$$D(t) = d \sin(\omega_m t + \chi) \tag{14}$$

This demodulation waveform is offset relative to the modulation waveform by an RF phase χ, and its amplitude d includes any gain or attenuation in the mixer. Multiplying (13) by (14) and disregarding all high frequency terms (ie. sum-frequency terms near $2\omega_m$ in the spectrum) gives the recovered signal component at a receiver located at the mixer output. Sum-frequency terms are filtered out, or integrated out by the receiver, in practice. The variance due to demodulated signal alone in the mixer output is:

$$\begin{aligned} \sigma_{sig}^2 = \; & 2\, d^2 E^4 \rho^2\, \alpha\,(1-\alpha)\, J_1^2(\phi_s/2)\, J_1^2(\theta_m) \cos^2\chi \\ & \times \left[a \sin^2(\phi_0/2 - \theta_0) + b \sin^2(\phi_0/2 + \theta_0) \right. \\ & \left. +2\,(ab)^{1/2} \sin(\phi_0/2 - \theta_0) \sin(\phi_0/2 + \theta_0)\right] \end{aligned} \tag{15}$$

Clearly it is important to select the correct demodulation phase χ (by careful control of time delays). From now on, $\cos^2\chi = 1$ will be assumed.

The total variance at the mixer output also contains a shot noise component, resulting from the subtraction of two uncorrelated shot noise contributions (half of the shot noise from each detector, due to the action of the passive splitter/combiner):

$$\sigma_{shot}^2 = 2\, d^2\, e\, B \times [\langle I_1 \rangle + \langle I_2 \rangle] / 2 \tag{16}$$

Here B is the resolution bandwidth of the receiver used, and e is the fundamental electronic charge. There is no dependence on the demodulation phase χ, and only the long-term average photocurrents $\langle I_1 \rangle$ and $\langle I_2 \rangle$ are important in calculating shot noise. Substituting (8) into (16) gives :

$$\sigma_{shot}^2 = d^2 e B E^2 \rho \left[(1-\alpha) + \alpha (a+b)/4 + \alpha /2 (ab)^{1/2} J_0(\phi_s) \cos(\phi_0) \right] \qquad (17)$$

Electronic noise due to detectors and amplifiers must also be considered when evaluating the total noise at the receiver, and this can be expressed as a noise variance after the mixer:

$$\sigma_{elec}^2 = d^2 e B E^2 \rho \varepsilon \qquad (18)$$

Here, ε is the ratio of the measured electronic noise after the mixer to the shot noise which would be observed at the same place if all of the optical power entering the interferometer was incident on the detectors (eg. set $\alpha = 0$ in (17)) . We have chosen to scale electronic noise in this manner for experimental and mathematical convenience. Note, ε depends not only on electronic noise, but scales inversely with input optical power.

There is a third noise component of interest in this scheme - laser intensity noise in the demodulated photocurrent spectrum. This noise component at the receiver is proportional to the subtracted photocurrent at frequency ω_m (see Equation (10)) as discussed above and is therefore sensitive to the operating phases θ_0 and ϕ_0. At the mixer output this ω_m component appears as a DC component surrounded by its related technical noise. The DC component can be approximated (setting $\sqrt{a} = \sqrt{b} = 1$) by:

$$I_{DC} = d\, 2\sqrt{2} E^2 \rho (\alpha (1-\alpha))^{1/2} J_1(\theta_m) \cos(\phi_0/2) \cos(\theta_0) \qquad (19)$$

With the associated technical noise variance given by:

$$\sigma_{tech}^2 = 8 RIN\, d^2 B E^4 \rho^2 \alpha (1-\alpha) J_1^2(\theta_m) \cos^2(\phi_0/2) \cos^2(\theta_0) \qquad (20)$$

where RIN is the relative intensity noise of the laser with respect to the DC component it is associated with. This noise will not be included in the general signal-to-noise expressions below - it turns out that at the optimum operating phases, this noise term vanishes.

2.6 Signal-to-Noise ratio in the demodulated output - general case

The signal to noise power ratio for the external modulation system is then given by $\sigma_{sig}^2 / (\sigma_{shot}^2 + \sigma_{elec}^2 + \sigma_{tech}^2)$:

$$S/N = 2E^2 \rho \alpha (1-\alpha) J_1^2(\phi_s/2) J_1^2(\theta_m) \times$$

$$\frac{a \sin^2(\phi_0/2 - \theta_0) + b \sin^2(\phi_0/2 + \theta_0) + 2 (ab)^{1/2} \sin(\phi_0/2 - \theta_0) \sin(\phi_0/2 + \theta_0)}{e B [\alpha (a + b)/4 + (1-\alpha) + \alpha /2 (ab)^{1/2} J_0(\phi_s) \cos(\phi_0) + \varepsilon]} \quad (21)$$

The signal-to-noise ratio in (21) is general for our configuration. However, we may simplify this expression by noting that only a few particular situations are of interest. We are aiming to optimise the signal-to-noise ratio by optimising the phases ϕ_0 and θ_0 in the Michelson and local oscillator beams, respectively, the modulation depth θ_m in the local oscillator arm, and the optical splitting ratio α.

Shot noise is minimised when $\phi_0 = \pi$ in the denominator, corresponding to a minimum in the Michelson output power. Putting this condition into (21) in turn demands that we select $\theta_0 = 0$ in the numerator to maximise signal power. This implies that at the detectors, the local oscillator field is optically in quadrature with the resultant field from the Michelson. The S/N varies with local oscillator phase like $\cos^2\theta_0$, when the Michelson phase is optimised. With the optimum optical phase settings throughout, equation (21) simplifies to :

$$S/N = \frac{4 E^2 \rho \alpha (1-\alpha) J_1^2(\phi_s/2) J_1^2(\theta_m) [1 + V] R}{e B [1 + \varepsilon - \alpha + \alpha R(1 - V J_0(\phi_s))/2]} \quad (22)$$

where $R = (a+b)/2$ is the mean power reflectivity of the Michelson interferometer mirrors and $V = (a\,b)^{1/2}/R$ is the fringe visibility of the Michelson interferometer.

2.7 Deviations from the ideal interferometer: Signal-to-Noise penalties

Practical interferometers will never operate exactly at the desired phase all of the time, due to experimental conditions (eg. vibrations and thermal drifts)resulting in an RMS phase error. The effects of this phase error can be analysed by adding technical noise to (21) and making the simplifying assumption that a = b = 1 resulting in:

$$S/N = \frac{8 E^2 \rho \alpha (1-\alpha) J_1^2(\phi_s/2) J_1^2(\theta_m) \sin^2(\phi_0/2) \cos^2(\theta_0)}{eB[1 - \alpha/2(1 - J_0(\phi_s) \cos(\phi_0)) + \varepsilon + 8 RIN/e\ E^2 \rho \alpha (1-\alpha) J_1^2(\theta_m) \cos^2(\phi_0/2) \cos^2(\theta_0)]} \quad (23)$$

We can then examine the sensitivity of (23) to phase errors in the Michelson by plotting the S/N as a function of phase ϕ_0, for a small signal $\phi_s \ll 1$ assuming that the local oscillator phase is optimally fixed $\theta_0 = 0$. In Fig 2, the effect of different levels of laser intensity noise is demonstrated - the higher the intensity noise, the smaller the tolerable RMS phase deviation. For signal frequencies around the laser relaxation oscillation frequency (~300 kHz), our laser restricts us to curve e in Fig 2, and hence requires an RMS phase error of less than 100 μradians in order to achieve maximum signal-to-noise performance. Fortunately the relative intensity noise of our laser is strongly frequency dependant and falls off rapidly above and below the relaxation frequency. Curve c for instance, corresponds to a signal frequency of approximately 500 kHz while at 2 MHz, where all quantitative tests were performed, the maximum RMS phase error that can be tolerated is in excess of 10 mradian (curve b Fig(2)).

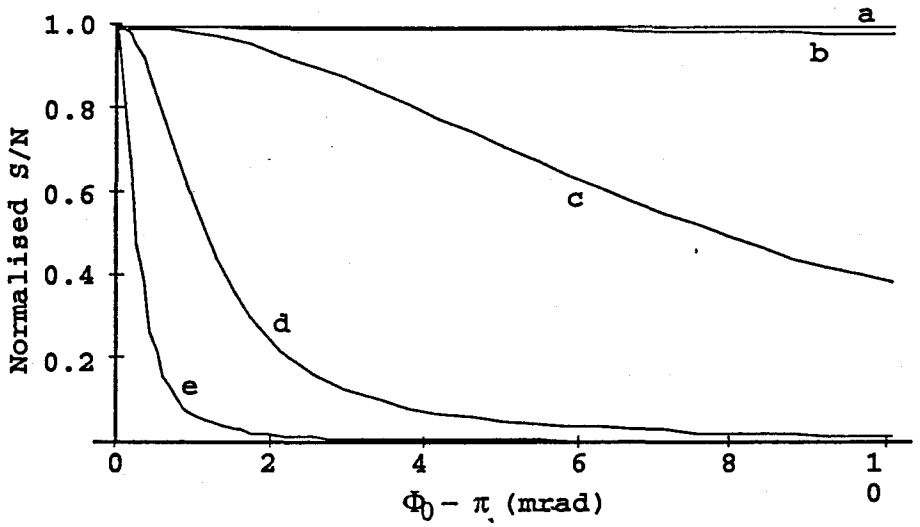

Figure 2: Normalised signal-to-noise power ratio verses dc Michelson phase ϕ_0, from (23), assuming the lo phase θ_0=0 and R = V = 1 (perfect optics) for variouse levels of laser relative intensity noise : **a**, RIN=0 (shot noise limited laser); **b**: RIN = 1×10^{-14}; **c**: RIN = 1×10^{-12}; **d**: RIN = 0.5×10^{-10}; **e**, RIN = 1×10^{-9}.

A tradeoff occurs between power tapped off into the local oscillator (which boosts the frequency shifted signal strength) and power lost from the Michelson (which reduces the original signal). The frequency shifted signal strength is proportional to $\alpha(1-\alpha)$, and is optimal when $\alpha = 0.5$. However, tapping off light into the local oscillator leads to extra shot noise at the detectors. In an ideal configuration, this is the only noise term, and S/N is actually optimum when $\alpha \rightarrow 1$. When unrelated noise is present, e.g. electronic noise, the optimum α falls somewhere between 0.5 and 1.

This trade-off between signal and local oscillator beam power is illustrated in Figure 3(a), which plots normalised signal to noise from (22) against the optical splitting ratio α, for different amounts of electronic noise ε, assuming all other parameters are optimised. In the ideal case of no electronic noise, $\varepsilon = 0$, curve 3(a) appears to rise linearly and approach its optimum at $\alpha = 1$. (In fact, the signal to noise drops sharply to 0 in a very small range close to $\alpha = 1$, because there is a

non-zero shot noise due to signal-related optical transmission in the Michelson.) Figure 3(b) plots the optimum value of α in an optically ideal interferometer as a function of electronic noise as well as the associated S/N ratio. The greater the electronic noise, the more power must be tapped off into the local oscillator arm to optimise sensitivity, but the worse that optimum becomes. Therefore it is experimentally prudent to use electronically quiet detectors/amplifiers or increase the input laser power (both operations reduce ε).

2.8 Signal-to-Noise ratio for small signals in the ideal limit

In general, we are interested in detecting extremely weak signals. In the limit $\phi_s \ll 1$, we may use Bessel function small argument approximations: $J_0(\phi_s) \to 1$ and $J_1^2(\phi_s/2) \to \phi_s^2/16$. Substituting these approximations into (22) yields:

$$S/N = \frac{E^2 \rho \alpha (1-\alpha) \phi_s^2 J_1^2(\theta_m) [1 + V] R}{4 e B [1+\varepsilon-\alpha+\alpha R(1- V)/2]} \qquad (24)$$

When the mirrors are both close to perfect R and V approach 1. Equation (24) is useful for comparison to measured signal-to-noise, because each of the independent physical parameters can be determined experimentally.

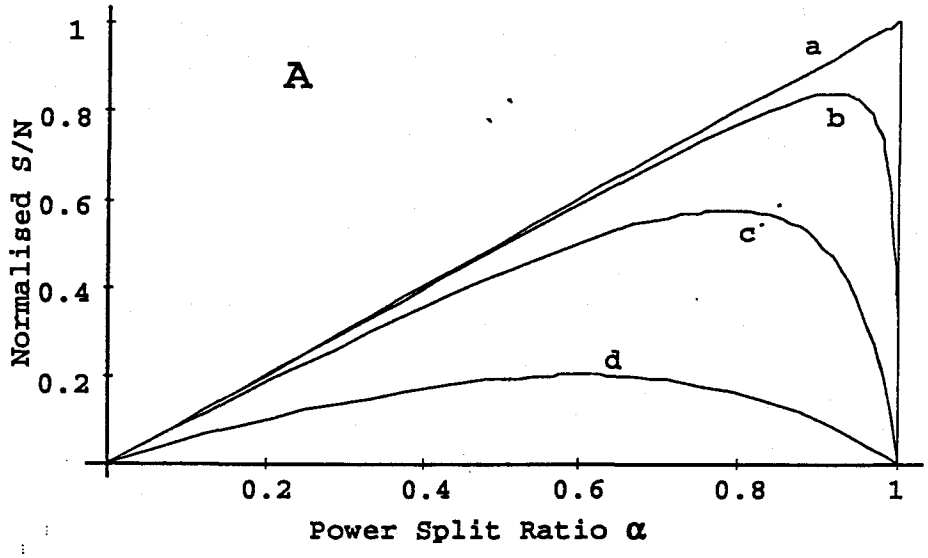

Figure 3 (a): Normalised signal-to-noise power ratio verses optical split ratio α, for various levels of electronic noise ε assuming perfect optics (R = V = 1): a, $\varepsilon = 0$; b, $\varepsilon = 0.008$; c, $\varepsilon = 0.08$; d, $\varepsilon = 0.8$.

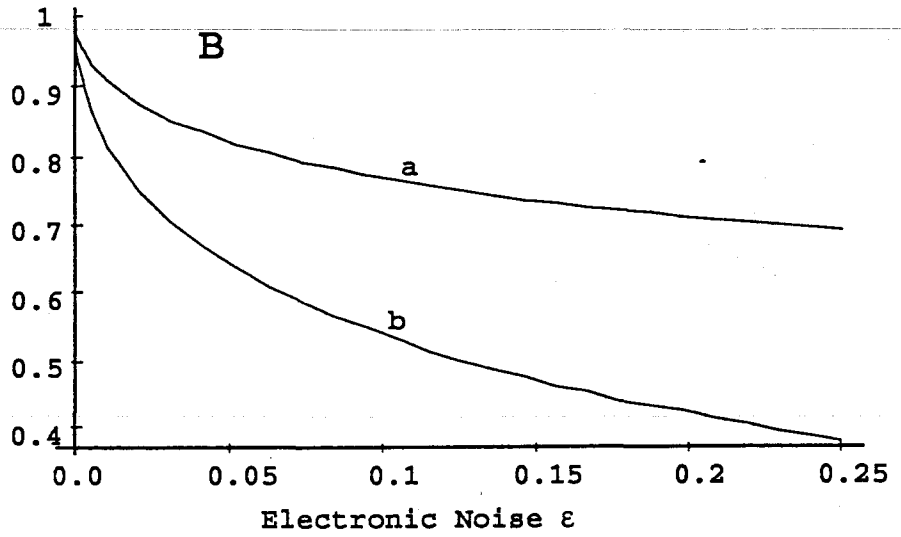

Figure 3 (b) : Curve "a": Optimum optical power split ratio α verses electronic noise assuming ideal optics (R = V = 1). Curve "b": The resulting signal-to-noise ratio when the optimum value of α (given by curve "a") is used, verses electronic noise ε.

The modulation depth θ_m in the external arm is an independent variable and can be set to maximise $J_1^2(\theta_m)$ when $\theta_m = 1.84$ radians. In this case $J_1^2(\theta_m) = 0.338$. Experimentally this is achievable using a resonant Pockels cell, but the required crystal is long, often producing significant wavefront distortions. Larger modulation depths lead to more power being transferred to higher order sidebands, not utilised by the demodulation process.

Assuming an ideal interferometer (ie., no electronic noise, $\varepsilon = 0$, perfect Michelson interferometer fringes, R = 1, V = 1 and optimum modulation $\theta_m = 1.84$ radians in the external arm) we have

$$(S/N)_{ideal} = 0.338\, E^2 \rho\, \phi_s^2\, \alpha / 2\, e\, B \qquad (25)$$

Here, it is apparent that to optimise the signal to noise ratio, we need to set α as large as possible, ie. $\alpha \rightarrow 1$. In this ideal limit,

$$(S/N)_{ideal} \rightarrow 0.676\, [E^2 \rho\, \phi_s^2 / 4\, e\, B] \qquad (26)$$

Equation (26) is in agreement with previous literature[1,2]. The factor in the brackets is the S/N limit which would be achieved if an ideal *Direct Detection* scheme had been used[3].

$$(S/N)_{direct} \rightarrow E^2 \rho\, \phi_s^2 / 4\, e\, B \qquad (27)$$

The penalty (1.7dB on the log scale) relative to direct detection can be interpreted as the effect of inefficiencies inherent in the simple signal recovery process modelled here (single frequency modulation and demodulation). In principle, it is possible to construct a more complex modulation

scheme (involving higher harmonics) which can approach the direct detection limit, with 0.676 in (26) replaced by unity [4].

It is also noteworthy that the signal to noise obtained by the *Internal Modulation* technique is very close to that in (26) above:

$$(S/N)_{internal} \rightarrow 2/3 \left[E^2 \rho \phi_s^2 / 4 e B \right] \qquad (28)$$

where the penalty in that case is due to demodulation of non-stationary shot noise[5]. The decision to use external modulation rather than internal modulation must be based therefore on technical considerations rather than inherent sensitivity limits.

3. Experimental Configuration

A schematic of our experimental external modulation arrangement, detailing the principal electronic and optical components, is shown in Fig 4. This configuration closely matches that of the model analysed in the previous section.

3.1 Optical configuration

The lightsource is a "MISER" Nd:YAG CW laser (Lightwave Electronics model 120) operating at 1064 nm. The output beam is directed through a Faraday isolator and then into a variable beam splitter consisting of a rotatable half wave plate and a polarising beam splitter . The vertically polarised output from the variable beam splitter traverses a lens and then enters the Michelson sensing interferometer.

A Pockels cell in one arm of the Michelson interferometer provides a small, calibrated, optical phase "signal", while a neutral density filter in the other arm provides optical amplitude compensation to obtain good fringe visibility at the Michelson output. By this technique, we are able to obtain a fringe contrast in the Michelson of around 600:1 (fringe visibility V = 0.9967). The factor ultimately limiting contrast is wavefront distortion in the Pockels cell.

The local oscillator beam emerges with an orthogonal polarisation to that of the Michelson beam and so another half wave plate is used to rotate the polarisation state by 90°. The variable beam splitter allows experimental adjustment of the power splitting ratio α by rotation of the initial half wave plate.

Under normal operating conditions, the Michelson interferometer is locked so that the output port is tuned to a dark fringe. The optical power injected into the Michelson interferometer is then reflected back toward the laser. It proved necessary to misalign the Michelson reflected beam slightly to prevent it re-entering the laser, as the 30dB Faraday isolator alone was insufficient to

prevent laser oscillations due to optical feedback. These were particularly observable when the Michelson phase modulation (signal) frequency corresponded to the relaxation oscillation frequency of the laser (~ 300 kHz).

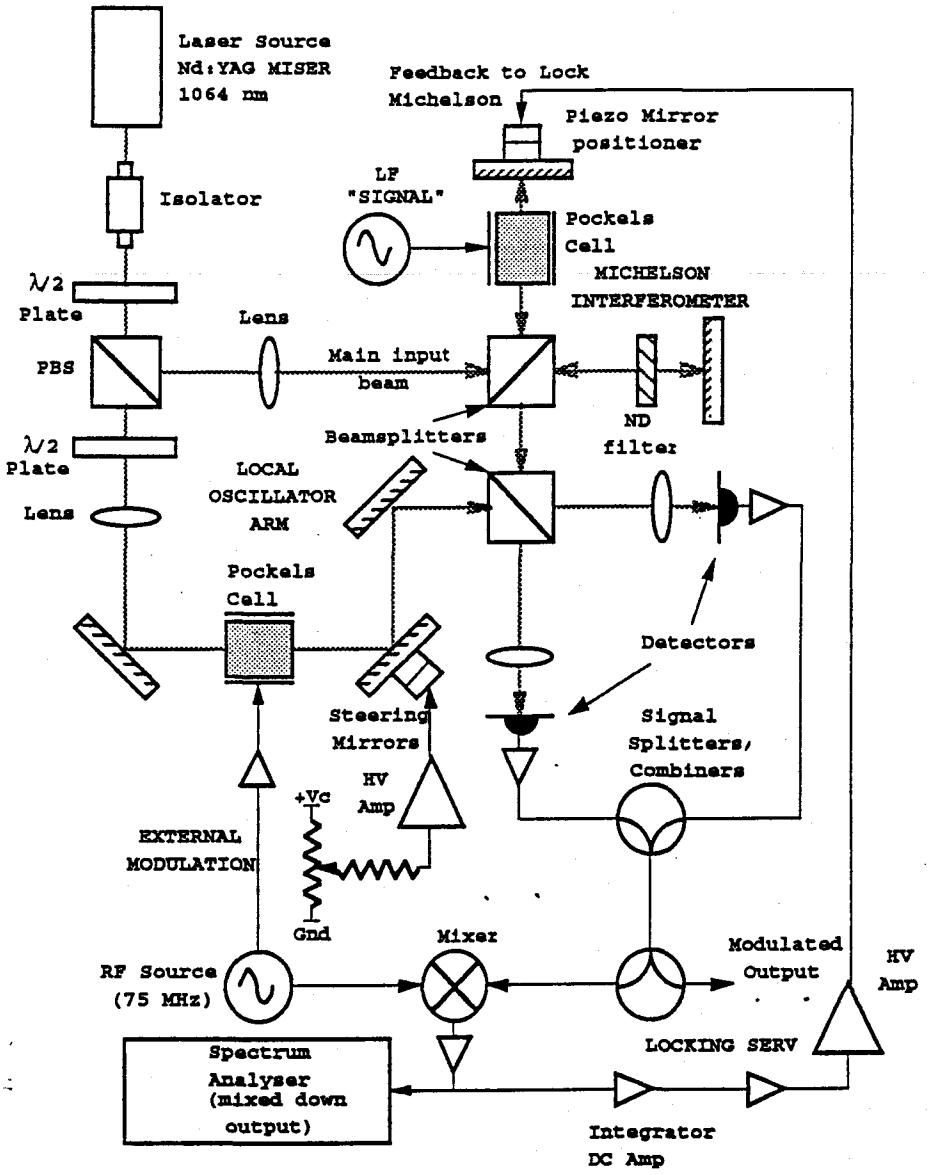

Figure 4: Detailed schematic of the external modulation interferometer experiment.

The local oscillator beam traverses a mode matching lens, a resonant Pockels cell (New Focus model 4003, resonant at 75 MHz) and is then directed into the final beam combiner via two steering mirrors. By adjusting the control voltage on the piezo actuator, the relative phase of the local oscillator field can be tuned with respect to the Michelson output. The Michelson output beam and the local oscillator beam are coherently combined at a 50:50 beam splitter, and the two outputs are focussed onto a balanced pair of detectors. The best obtained fringe contrast for this Mach-Zehnder interferometer (measured by combining the local oscillator beam with an equal intensity beam from

just one arm of the Michelson interferometer) was around 150:1, limited by wavefront distortion in the resonant Pockels cell. This is more than adequate to ensure near optimal operation.

The Michelson end-mirrors in each arm are placed to ensure accurate matching of the two Gaussian beams at the output of the Michelson. It should be noted that matching the spot-sizes and wavefront curvatures of two beams does not necessarily correspond to matching their absolute optical path lengths. Geometric factors in one arm of the interferometer, such as refraction in a high-index element such as the Pockels cell, can mean that it is necessary to shorten the other arm (rather than lengthen it as intuition might suggest) to correctly match the two Gaussian output beams. Note: This will unavoidably introduce an optical path length mismatch, comparable to the length of the Pockels cell.

The primary purpose of the lens in the local oscillator beam is to create a beam-waist inside the resonant Pockels cell, but this necessitates an identical lens in the Michelson input beam, placed so that both beams arriving at the final beam combiner experience the same optical evolution. It proves more effective to match the beam evolutions as closely as possible in the first instance than to correct for different beam paths subsequently with extra lenses.

3.2 Electronic configuration

The light is focussed onto a pair of balanced InGaAs detectors (Epitaxx ETX500) AC coupled via a 50Ω linear amplifier, with a flat frequency response from about 6 MHz to 250 MHz. The output voltages are subtracted by a passive 180° signal combiner to coherently combine signals from both detectors, yielding a 3dB improvement in the attainable signal-to-noise ratio (since the shot noise from each detector is uncorrelated).

The output from the passive signal combiner is itself split at a passive signal splitter and one output is fed directly to a receiver (a Hewlett Packard HP8568B spectrum analyser) while the other is mixed down to recover the original signal spectrum using an RF mixer. The local oscillator for the mixer is derived from the external modulation signal source at 75 MHz, with an appropriate time delay to optimise the demodulation phase (χ in Section 2). This RF electronic operation was modelled in Section 2 by multiplying equations (13) and (14). Experimentally the signal-to-noise is independent of the mixer gain d, in accordance with Equation (19). There is also a 3dB gain in S/N (when the correct demodulation phase is chosen) because frequency convolution combines coherent signal sidebands and incoherent noise sidebands. The demodulated signal spectrum is fed to the receiver (HP8568B), and also acts as an error signal for locking the Michelson interferometer.

Electronic noise arising in the detectors and amplifiers is characterised by ε, as defined in Equation (18). This is determined experimentally by measuring the electronic noise directly at the mixer output and comparing it to the shot noise measured at the same point for a given optical power incident on the detectors. Since Equation (18) normalises electronic noise to the maximum possible shot noise level (which would be observed if all the light was incident on the detectors), it is

necessary to scale up the measured shot noise appropriately to account for this definition. In this manner we obtain values of $\varepsilon \sim 0.08$ for an effective total optical power of 9mW.

To reduce vibration-induced RMS phase excursions from the Michelson dark fringe (and hence to reduce the amount of optical transmission and associated technical noise from the laser), it is necessary to actively lock the Michelson to the dark fringe. Interferometric phase locking is achieved by integrating the error signal, and amplifying the result to drive a piezo-controlled mirror in one arm of the Michelson. The desired locking condition is complete nulling of the 75 MHz component in the subtracted photodetector output, which corresponds uniquely to a dark fringe in the Michelson interferometer, but good 75 MHz cancellation is only achieved when the local oscillator optical phase is approximately correct. This local oscillator phase is set by manually tuning the piezo mirror in the local oscillator arm. When the feedback loop is active, locking follows automatically as soon as the local oscillator is within ~45° of the correct phase; subsequent fine tuning of the local oscillator phase optimises the demodulated signal at the receiver.

The response of the integrator, the following amplifiers and the piezo mirror mount combine to produce an open loop unity gain at around 5 kHz. This is sufficient to counteract differential acoustic and vibrational noise in the interferometer so that laser technical noise appearing in the demodulated output spectrum is suppressed by more than 50 dB under normal operating conditions .

4. Experimental Results

4.1 Motivation for these experiments:

The simple model of a non-ideal external modulation system analysed in Section 2 is only worthwhile if it can genuinely describe a realistic experimental interferometer. It is necessary to perform a series of experiments to verify the predictions of the theory (or otherwise), to determine whether or not we have included sufficient (or superfluous) non-ideal features in the model. Experimental measurements will also reveal technical issues which the model cannot predict, such as potential difficulties in operating a practical instrument, or the relative sensitivities of the device to various technical noise sources such as acoustic disturbances.

4.2 Locking the interferometer

To confirm the experimental predictions of our generic model of the external modulation scheme in Section 2, it is first necessary to lock both the Michelson interferometer and the local oscillator beam to their correct operating phases. Manual locking is sufficient in the local oscillator arm because the final sensitivity depends only weakly on the local oscillator phase (S/N varies like $\cos^2\theta$ in Section 2). In the benchtop Michelson interferometer, on the other hand, manual locking to a dark fringe is completely ineffective, as acoustic and low frequency mechanical vibrations produce a significant RMS differential phase error. This leads to a certain amount of unwanted

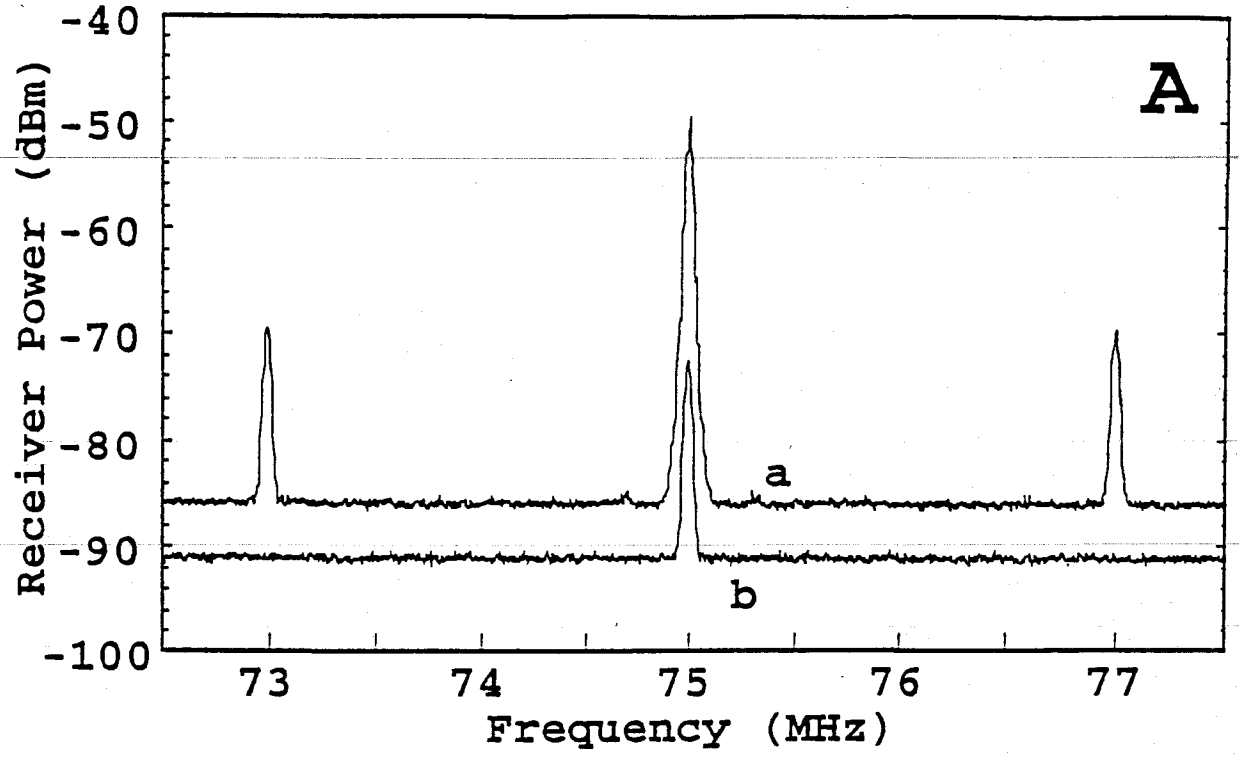

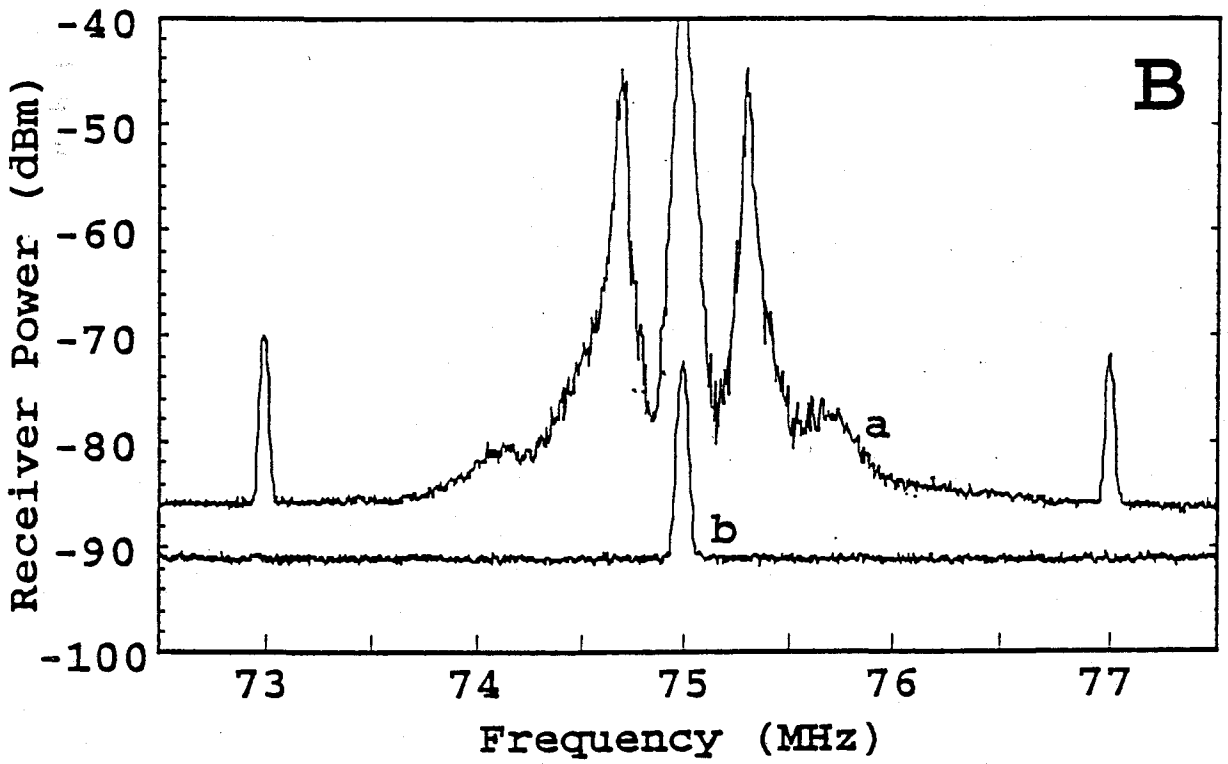

Figure 5 (a): Curve "a" shows 2MHz signal sidbands and residual 74.9MHz modulation component when locked using 5kHz servo system. Curve "b" shows the electronic (dark) noise. (b): As in (a) with servo system turned off and manual locking used. (c): The corresponding sperta to (a) at the mixer output. (d): The corresponding sperta to (b) at the mixer output. All spectra recorded with RBW = 30kHz, vbw = 30Hz while the optical power on each detector is ~1mW

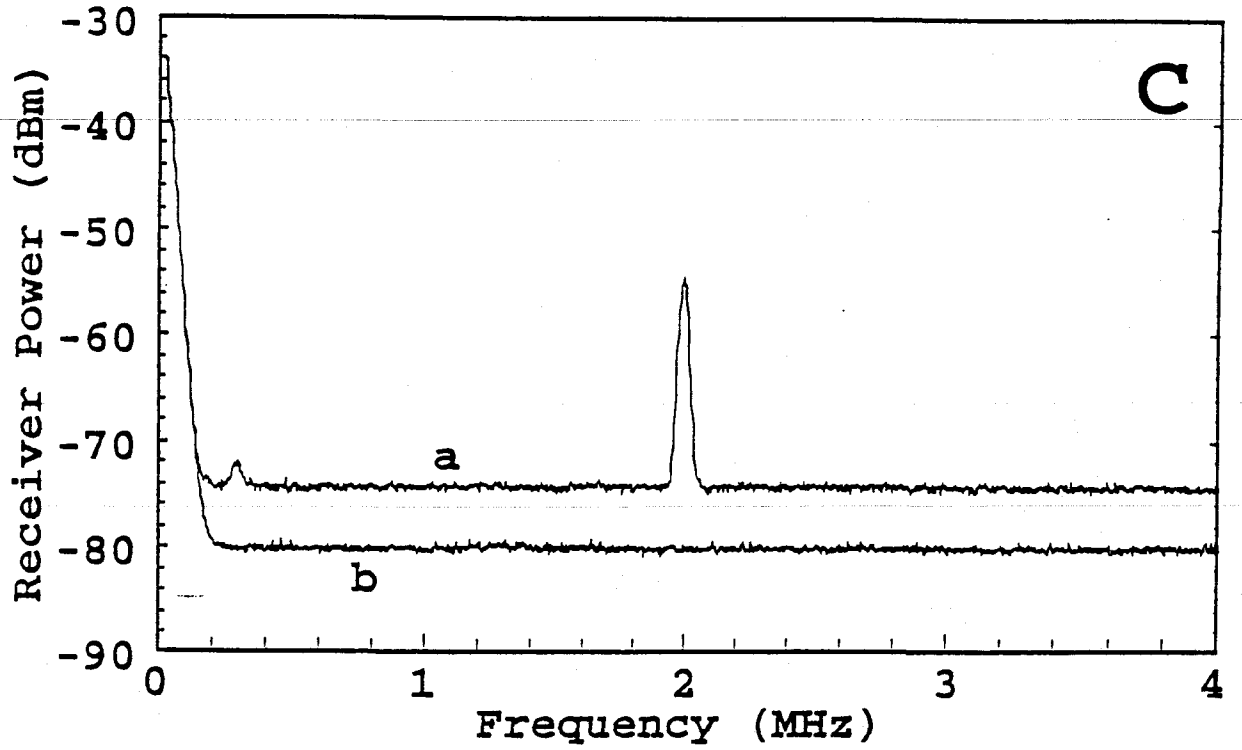

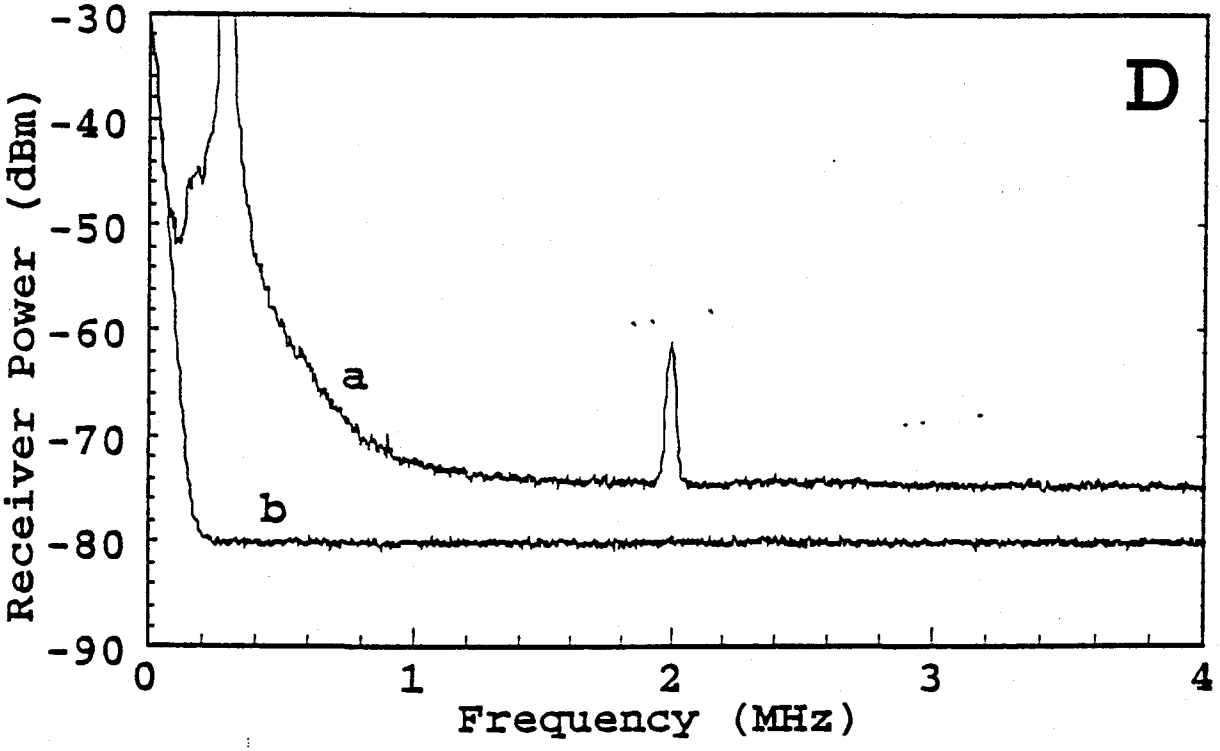

Figure 5 (c): The corresponding sperta to (a) at the mixer output. (d): The corresponding sperta to (b) at the mixer output. All spectra recorded with RBW = 30kHz, vbw = 30Hz while the optical power on each detector is ~1mW

optical transmission, unimportant in its own right, but laser intensity noise associated with this unwanted light appears in the frequency-shifted signal spectrum, easily obscuring small signals and shot noise at low frequencies. It is therefore essential to employ an active locking system, such as the servo loop used here.

To demonstrate the difference between the performance of the interferometer with passive (manual) nulling and active (feedback) locking, Figure 5 shows the simultaneous signal and noise spectra obtained at the receiver, in both cases, for a strong signal near 2 MHz. For clarity, frequency-shifted signals measured at the mixer input (Fig 5(a) obtained with active locking and Fig 5(b) with manual nulling) are compared to demodulated signals obtained at the mixer output (Fig 5(c) active locking and 5(d) manual nulling). These spectra highlight the origin of the demodulated laser intensity noise - it is present in the frequency-shifted photocurrent spectrum, and therefore cannot be post-filtered to reveal the signal spectrum after detection.

The unwanted intensity noise obtained with manual locking is orders of magnitude larger than shot noise, even when the interferometer is held as closely as possible to a dark fringe. Indeed, during the 10 seconds required to record each single spectral scan on the analyser, the observed technical noise varied by ±10dB typically, due to small uncontrolled phase excursions from the dark fringe.

Prominent on the manually locked spectra are the relaxation oscillation peaks of the Nd:YAG laser 300 kHz either side of the 75 MHz carrier residual in the frequency shifted spectrum, Fig 5(b), and near 300 kHz in the demodulated spectrum Fig 5(d). Large wings associated with the relaxation peaks extend to higher frequencies in both traces. Only active feedback compensation of the mechanical noise in the interferometer with a broad-band, high-gain control loop enables us to observe signals at the shot noise limit at low frequencies (down to around 80 kHz, in practice, below which laser frequency noise dominates; see below for discussion).

Fig 5 also shows another feature, mentioned in the previous section - a 3 dB improvement in the signal to noise ratio in the mixer output compared to that measured at the mixer input. In the actively-locked interferometer where technical noise is suppressed sufficiently to observe shot noise, the frequency-shifted signal sidebands at the mixer input are 16.6 dB above shot noise in Fig 5(a), while the demodulated signal is 19.7 dB above the demodulated shot noise floor in Fig 5(c).

4,3 Signal-to-noise measurements

To confirm the quantitative predictions of the analysis in Section 2, we conducted a series of signal-to-noise measurements in the interferometer, for small phase modulation signals at ~2 MHz, imposed on one beam of the Michelson interferometer. In each one of these tests, we measured the following independent system parameters for substitution into the signal-to-noise Equation (24), to derive the expected signal-to-noise ratio for each measurement:

- Photocurrents in both detectors due to the Michelson bright and dark fringes and the local oscillator beam separately; From these are derived the effective total input, $E^2\rho$, the experimental optical splitting ratio α and the Michelson fringe visibility V. (For convenience, R is set to unity in (24), with Michelson transmission losses subsumed into the effective total input.)
- Electronic noise, and shot noise measured at the Michelson bright fringe, from which we derive the electronic noise parameter ε.
- Driving voltages in both calibrated Pockels cells, from which the signal phase ϕ_s and the external phase modulation depth θ_m are calculated.

In all cases, the resolution bandwidth B of the receiver was set to 10 kHz. The signal-to-noise ratio was measured directly at the receiver when the system was locked to a dark fringe and local oscillator phase was optimised. In most cases of interest, we obtained excellent agreement to the theoretical predictions of Equation (24).

4.4 Sensitivity tests - measurements of small signals

Fig. 6 shows a typical signal-to-noise spectrum obtained for a small signal equivalent to the sensitivity of the instrument. By definition, *the sensitivity is the phase modulation required to produce a demodulated signal equal in magnitude to the total demodulated noise,* ie. S/N = 1 in (24), or 3 dB (S+N / N = 2) on the spectrum analyser. From (24), the predicted sensitivity for the non-ideal external modulation scheme is :

$$\text{Sensitivity} = \left[4\,e\,(1+\varepsilon-\alpha+\alpha R(1-V)/2) \,/\, E^2\rho\,(1+R)J_1^2(\theta_m)\;\alpha(1-\alpha)\right]^{1/2} \qquad (29)$$

Here, the normalised sensitivity (radians/$\sqrt{\text{Hz}}$) is quoted by dividing the absolute sensitivity by the resolution bandwidth B. From (29), the maximum normalised sensitivity for an external modulation system is:

$$(\text{Sensitivity})_{max} = 0.676^{-1/2}\left[4\,e / E^2\rho\right]^{1/2} \qquad (30)$$

This is 21.6% worse than the maximum sensitivity for a direct detection system.

The top trace in Fig. 6 shows the demodulated signal peak near 2 MHz and the total noise floor (shot noise + electronic noise) when the signal ϕ_s was 2.8 μrad (0-peak); the external modulation depth θ_m was 0.68 radians (well short of the optimum 1.84 radians); the effective input optical power was 9 mW and the detector efficiency ρ = 0.77 amps/watt. In this case, 80% of the power was transmitted to the Michelson, ie. α = 0.8 (close to the required optimum of 0.83). The fringe visibility of the Michelson, V, was 0.995. The lower trace of Fig. 6 shows the noise obtained when all light was blocked, ie. electronic noise alone, yielding ε = 0.08.

For these measured parameters, the predicted signal-to-noise was 2.98 dB. This represents a phase sensitivity of 2.8×10^{-8} rad/$\sqrt{Hz}$, equivalent to a displacement sensitivity of 4.7×10^{-15} metres/$\sqrt{Hz}$ at a wavelength of 1064nm.

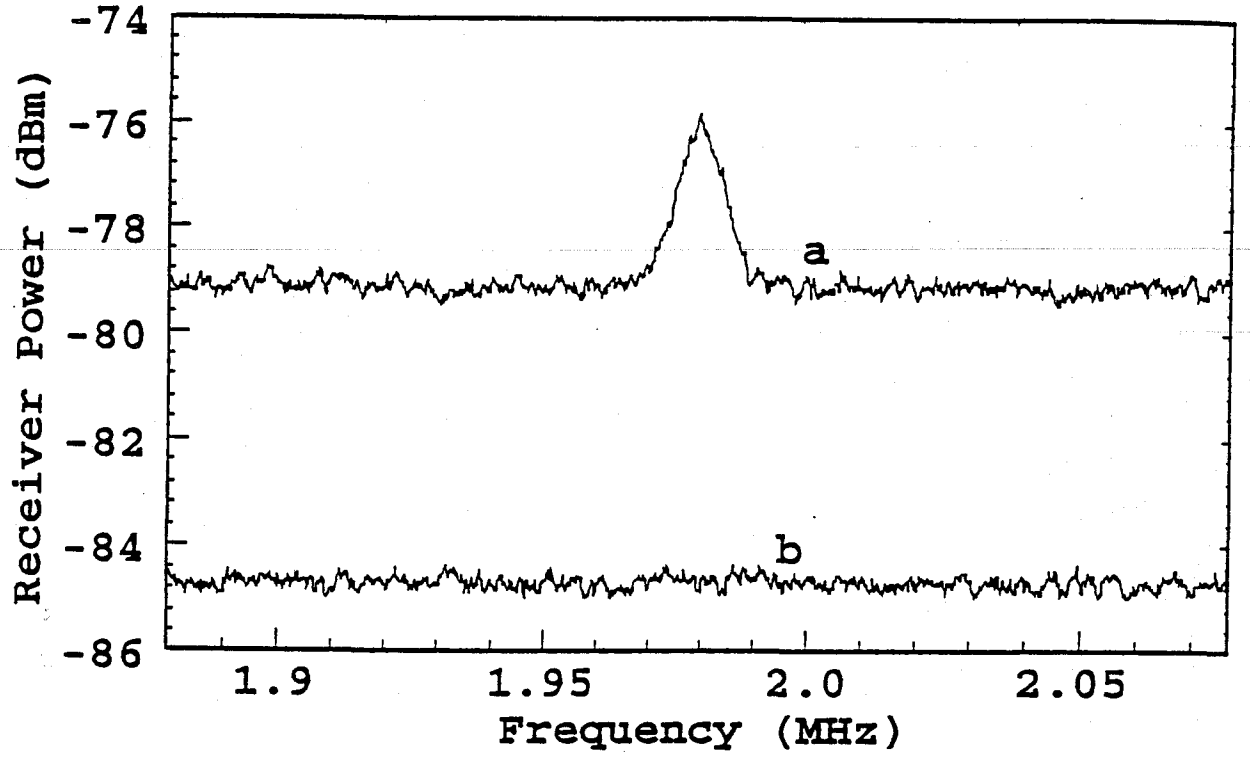

Figure 6: Curve "a" shows a small signal plus shot noise at the mixer output, demonstrating the sensitivity (3dB S/N) limit of the interferometer under the following conditions: RBW = 10kHz, VBW = 3Hz, detected optical power = 0.95 mW on each detector, effective input power = 8.9 mW, signal strength = 2.8 μradians, modulation depth of external beam = 0.68 radians. Curve "b" shows the electronic noise floor under the same conditions used in curve "a".

Fig. 7 plots the predicted sensitivity, using Equation (29), along with measured sensitivity from a series of trials in which the measured signal-to-noise was set to 3dB, as the external modulation depth θ_m is varied. Clearly, the sensitivity improves as modulation depth θ_m is increased. As the external modulation depth increases from 0.11 to 1.18 radians (0-peak), the displacement sensitivity improves by a factor of 7.6, from 2.6×10^{-14} m/$\sqrt{Hz}$ to 3.4×10^{-15} m/$\sqrt{Hz}$. Theory predicts that the sensitivity should increase by a factor ~9 due to this increased modulation, experimental error in our low RF power measurements accounts for the discrepancy.

4.5 Measurements with large signals

A related test to illustrate the signal-to-noise calculations in Section 2 is to apply a constant signal to the Michelson interferometer and measure the signal-to-noise ratio for different values of the external phase modulation depth. For this purpose, large signals are expected to yield the most

accurate results, since noise should have less effect on the absolute dB signal peak readings. Fig. 8 shows a spectrum analyser trace for a signal of 2×10^{-4} radians (0-peak), all other parameters being identical to those used to obtain Fig. 6. Here the measured signal-to-noise is 38.7 dB, compared to a predicted value of 37.0 dB from Equation (24).

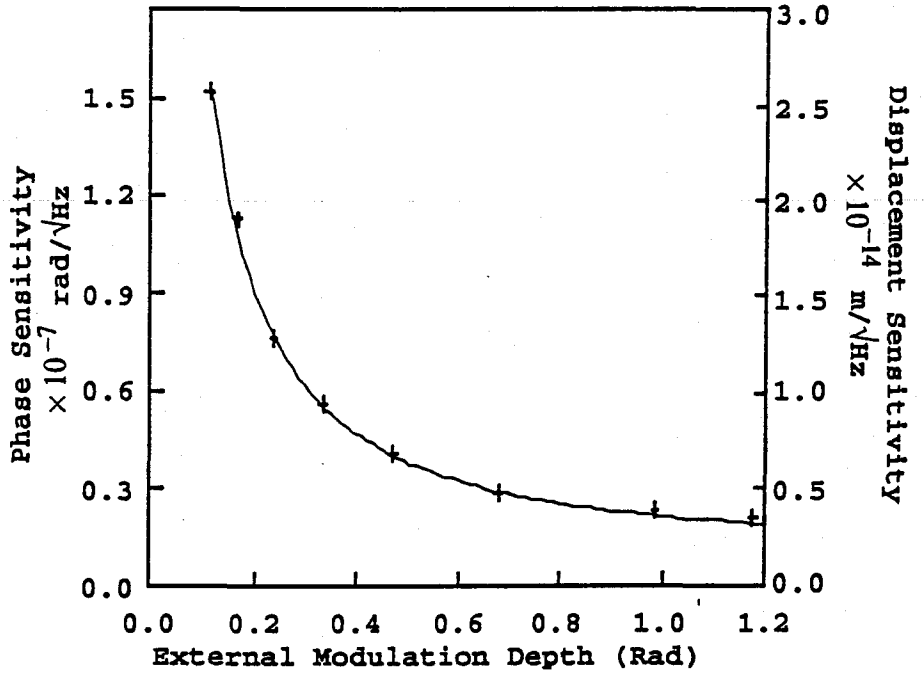

Figure 7: Experimentally achieved sensitivity (data points marked as crosses) verses external modulation depth for a 2MHz signal. For comparison the predicted theoretical sensitivity (solid line) is also plotted. The left hand scale gives the phase sensitivity in radians/√Hz while the right hand scale gives absolute displacement sensitivity in metres/√Hz.

Fig. 9 plots the signal-to-noise ratio obtained in a series of measurements using a constant signal strength of 2×10^{-4} radians (0-peak), and again we are varying the external phase modulation depth θ_m. In this case, the measured signal-to-noise consistently exceeds the predicted level from Equation (24) by between 1.4 and 2 dB.

It is apparent that there is excellent agreement between theory and experiment for small signals ($\phi_s \sim 1$ µrad or less) while for large signals ($\phi_s \sim 100$ µrad or more) there is a discrepancy of 1.4 to 2 dB. To investigate this transition from small to large signals, we held all other parameters constant and measured the signal-to-noise ratio as a function of applied signal strength. The smooth growth in the discrepancy between measured and predicted signal-to-noise ratios is demonstrated in Fig. (10). There is evidently a rapid and systematic onset of this discrepancy, with a growth initially of around 2 dB per decade of signal phase, levelling out eventually to a total discrepancy of ~ 2 dB for larger signals.

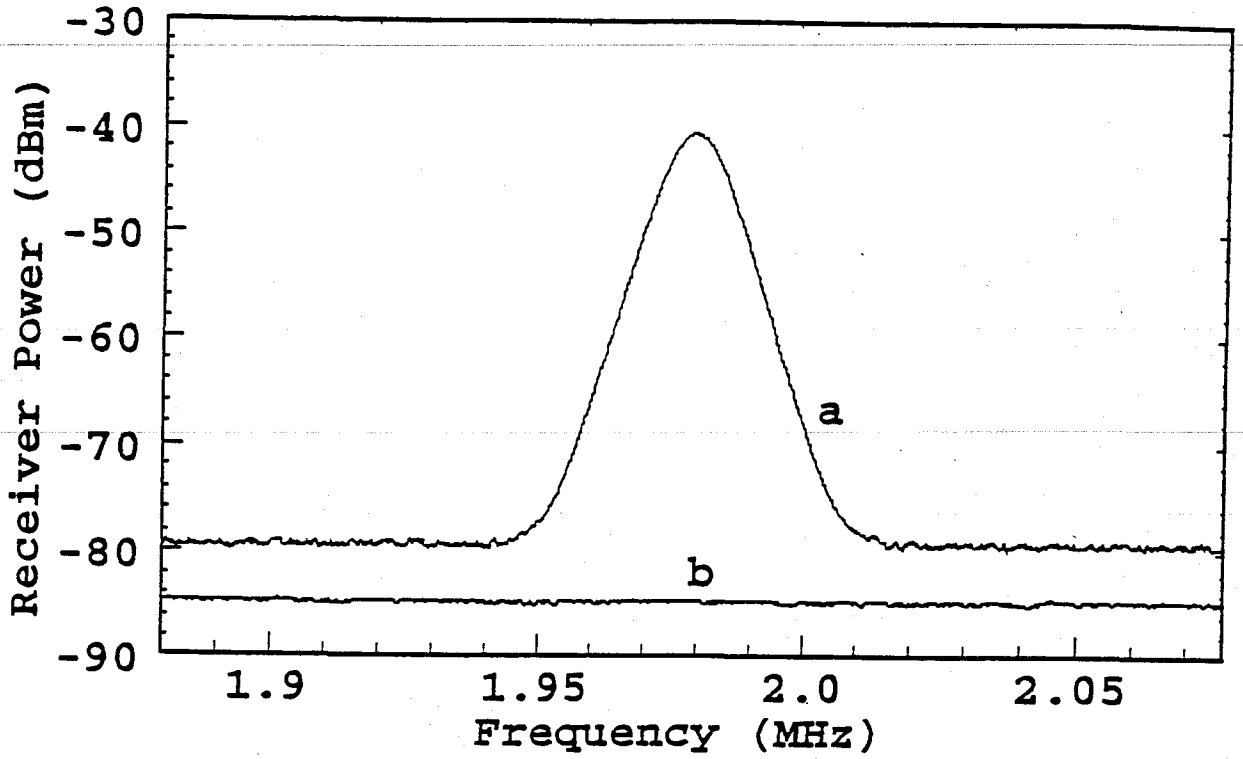

Figure 8: Curve "a" shows a large 2MHz signal plus shot noise at the mixer output under the following conditions: RBW = 10kHz, VBW = 3Hz, detected optical power = 0.95 mW on each detector, effective input powrer = 8.9 mW, signal strength = 200 μradians, modulation depth of external beam = 0.68 radians. Curve "b" shows the electronic noise floor under the same conditions used in curve "a".

The reason for this systematic discrepancy is not completely understood, but its origin can been isolated to some extent by eliminating obvious possibilities. Firstly, we noted during the measurements detailed in Fig. 10 that the noise floor did not vary with signal depth - the entire variation in Fig. 10 is due to the extra growth in signal strength. This alone is sufficient to eliminate electronic and detector saturation as a cause - such saturation could have led to a depressed noise floor and an apparent increase in the signal-to-noise ratio in certain frequency regimes. Furthermore, photodiode saturation is unlikely, because we are collecting only ~ 0.8 mW on each detector, an order of magnitude below the maximum allowed intensity.

Saturation of the amplifiers after the detectors seems unlikely, given that the cause could only be the large 150 MHz component in the photocurrent (the second harmonic of the modulation frequency when operating at the correct DC phase) - we are able to vary this by 20 dB while the discrepancy remains approximately constant. Problems in the RF mixer are an unlikely explanation, because we observed the standard 3.0 dB improvement in signal-to-noise after the mixer compared to that measured at its input.

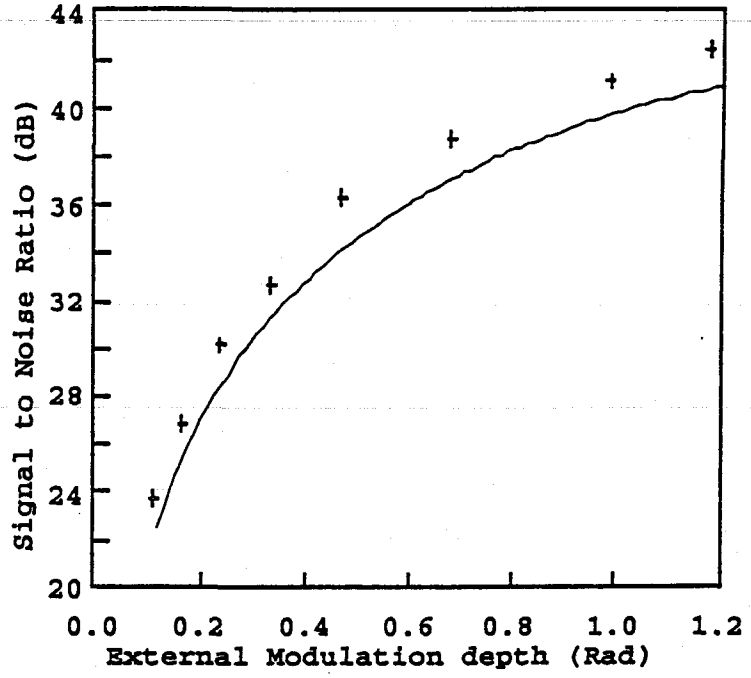

Figure 9: The experiementally achieved signal-to-noise ratio plotted as a function of the external modulation depth (data points are plotted as crosses). For comparison, the predicted signal-to-noise (solid curve) is also plotted.

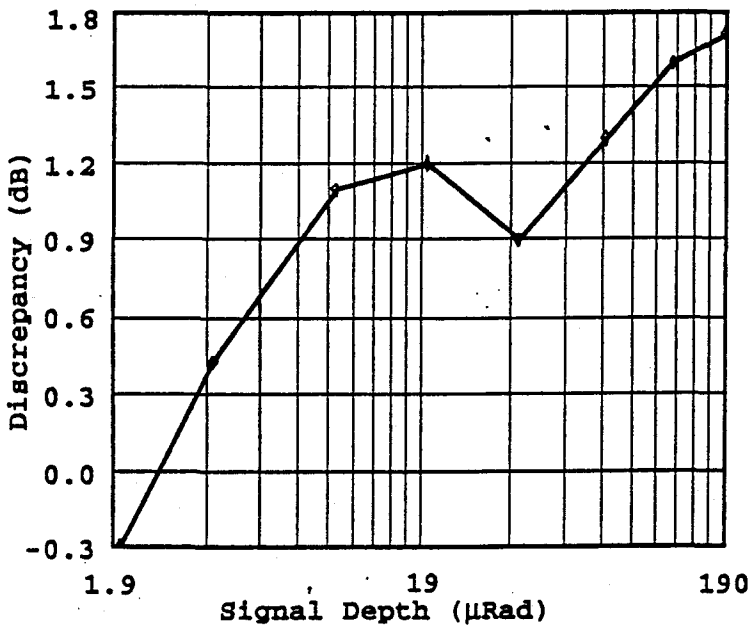

Figure 10: Discrepancy between experimental signal-to-noise and predicted signal-to-noise, plotted in dB, verses signal stength in radians.

We may be experiencing optical feedback from the Michelson interferometer to the laser. This possibility remains, despite the fact that we are using an Faraday isolator giving ~ 30dB isolation, as well as misaligning the return Michelson beam so that it illuminates a spot several spot radii

from the isolator aperture. The feedback, if it exists, can only be due to the phase modulation (as opposed to amplitude modulation) in the return beam from the Michelson (given that it is locked to a bright fringe when the output is locked to a dark fringe). If it is feedback we are observing, then it is phase noise (frequency noise) in the laser output that is responsible for the anomalies results. Amplitude noise, like the technical noise we have already cancelled, can not appear in the shifted signal spectrum of our external modulation system. This explanation is yet to be confirmed by further experiments.

4.6 Low frequency limits to shot-noise-limited sensitivity

The purpose of the external modulation technique is to eliminate laser intensity noise from the signal spectrum. The efficiency of the scheme relies on the ability of the servo loop to minimise the RMS phase deviation from the dark fringe - the smaller the RMS deviations, the greater the suppression of intensity noise. Because intensity noise is greatest at low frequencies, the use of better servo loops enables us to view shot noise limited signal spectra at lower frequencies.

In our experiment, intensity noise was suppressed by more than 50 dB, but despite this, we were not able to view shot noise in our demodulated signal spectrum below ~ 80 kHz. Between DC and ~ 100 kHz, a number of anomalous noise peaks remained, of variable strength, typically 10-20 dB greater than shot noise in the demodulated signal spectrum, apparently harmonically related and with a fundamental frequency of around 30 kHz.

Fig. 11(a) shows the anomalous noise in the frequency-shifted signal spectrum near 75 MHz, along with the deliberate signal peaks located 200 kHz either side of the residual carrier. Unlike the laser intensity noise, the magnitude of these extra noise peaks did not depend on the detuning from the Michelson dark fringe. Fig. 11(b) shows the same structure in the demodulated signal spectrum.

The origin of these unwanted noise peaks is frequency fluctuations in the laser, combining with optical path length differences in the two Michelson interferometer arms to simulate another "signal". Such a signal would disappear if the path lengths were perfectly matched, but in our experiment, the two-way path mismatch is around 60 mm, due to the need to match Gaussian modes at the beam combiner when one beam passes through a Pockels cell. From rough calculations, the observed peaks are consistent with a phase noise spectral density of around 3 mrad/$\sqrt{\text{Hz}}$ at 30 kHz. This could arise, for example, due to an acoustic resonance causing the laser cavity round-trip path to fluctuate. Independent frequency noise tests of our laser, using a reference cavity and Pound-Drever locking confirm that frequency noise of around 3 mrad/$\sqrt{\text{Hz}}$ at 30 kHz does exist on the laser however the exact origin of this noise is not yet certain.

5. Conclusions

External modulation has been shown to be a viable technique for extracting shot noise limited signals from spectral regions dominated by laser intensity noise. We have presented a simple analytic model which includes several non-ideal features likely to be encountered in any practical

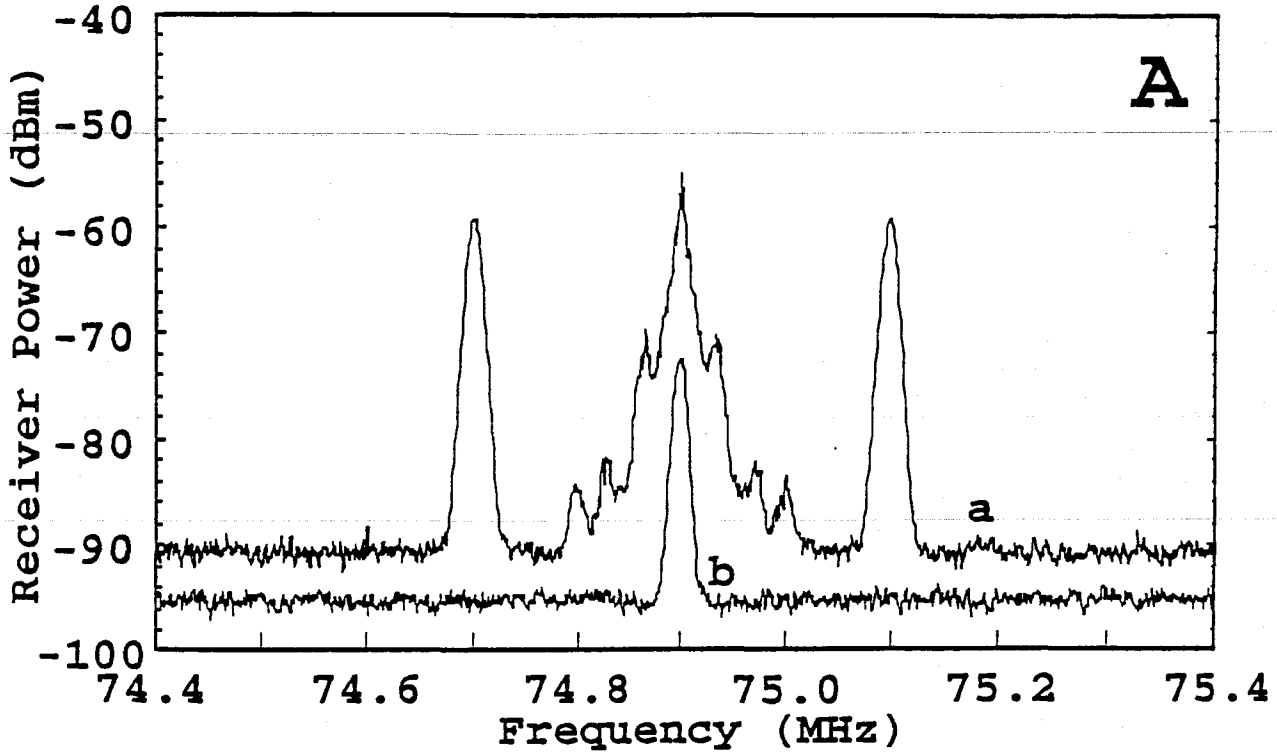

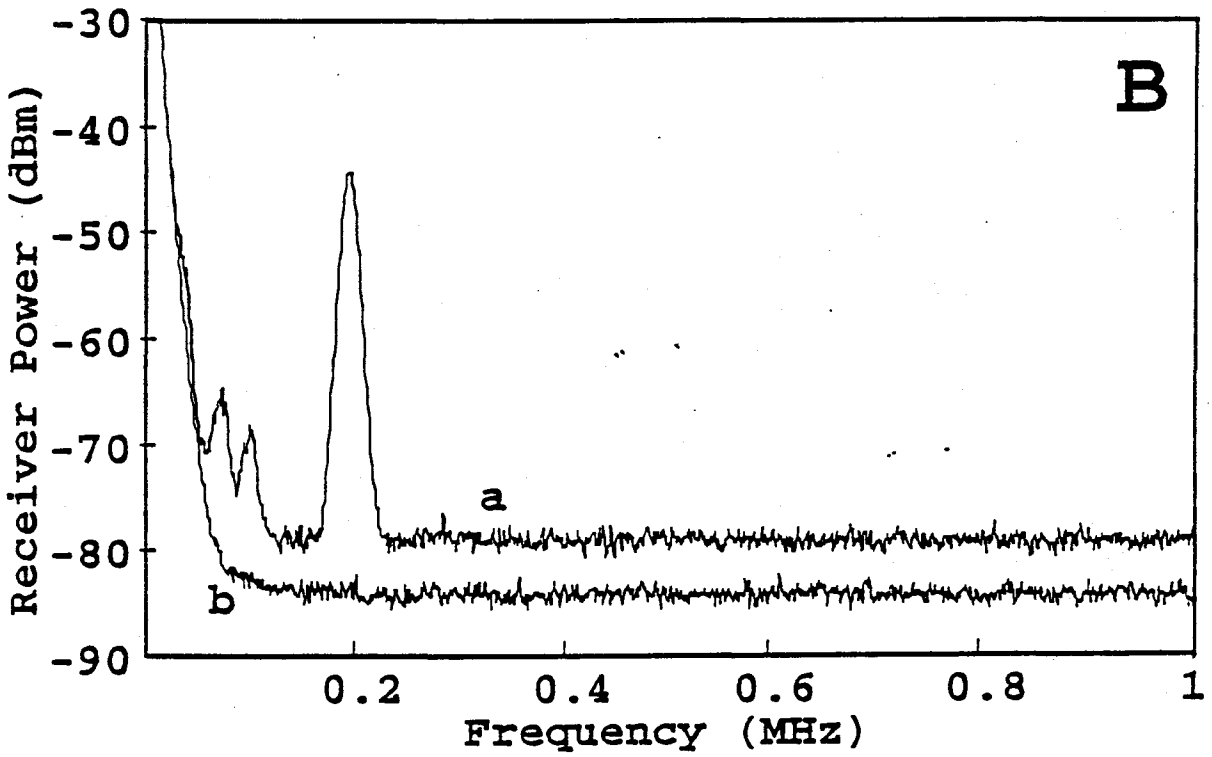

Figure 11(a): Curve "a" shows the spectrum of low frequency signal sidebands, the 74.9MHz modulation component and low frquency technical noise at the mixer input. Curve "b" shows the electronic noise floor at the mixer input (also demonstrating the mixer feedthrough occuring at 74.9MHz).

(b): Curve "a" shows the spectrum of low frequency signal and technical noise at the mixer output. Curve "b" shows the electronic noise floor at the mixer output.

realisation of this scheme. The principal features of this model are the controllable optical tap-off ratio for the local oscillator beam, the assumption that the sensing (Michelson) interferometer does not produce perfect optical fringes, and the inclusion of electronic noise from the detectors and amplifiers. The key predictions of this model are:

- It is possible to suppress technical noise from a laser in the detected signal spectrum to make shot-noise-limited measurements of low frequency signals otherwise unobtainable via direct detection.

- The interferometer should be operated so that the Michelson interferometer is locked to a dark fringe as closely as possible to prevent laser intensity noise appearing in the demodulated signal spectrum.

- Locking to a dark fringe also minimises shot noise in the demodulated signal and maximises the signal strength.

- The external beam should be phase modulated with a 0-Peak modulation depth of 1.84 radians to optimise the strength of the recovered signal.

- The local oscillator beam should be phase locked so that it is optically in quadrature with the resultant field emerging from the Michelson for maximum signal sensitivity.

- The optical tap-off ratio to the local oscillator beam is ideally close to zero - ie. all power should go via the Michelson interferometer, but the existence of electronic noise and shot noise due to imperfect Michelson dark fringes necessitates a finite tap-off fraction to optimise the signal-to-noise ratio. The greater the electronic noise or dark fringe transmission, the greater is the required tap-off fraction and the worse is the achievable sensitivity.

- The ultimate achievable sensitivity in an ideal external modulation system is comparable with that of internal modulation, and both schemes suffer ~ 33% sensitivity penalty compared to ideal shot-noise-limited direct detection, when simple modulation and demodulation waveforms are used.

We have also tested our theoretical predictions by constructing and making measurements with a simple benchtop Michelson interferometer with a local oscillator tapped off from the input beam. We verified the basic predictions of the analysis to within a few percent for small signals; a phase sensitivity of ~ 0.2 μrad/$\sqrt{\text{Hz}}$ equivalent to a displacement sensitivity of ~ 3.4 $\times 10^{-15}$ m/$\sqrt{\text{Hz}}$, using an input optical power of 9 mW, an external modulation depth of 1.2 radians (suboptimal), and a tap-off fraction of 20% to the local oscillator beam (close to optimal). For larger signals (200 μrad 0-Peak), there was a systematic and unexplained discrepancy of around 1.7dB in the signal-

to-noise ratio, possibly due to optical feedback effects between the Michelson interferometer and the laser.

Shot noise limited sensitivity was obtained for signal frequencies above about 100 kHz. Below this, frequency noise of the laser dominated the demodulated signal spectrum. This shot-noise-limited performance was obtained using an integrating servo loop with a bandwidth of around 5kHz to actively compensate acoustic and mechanical vibrations in the Michelson interferometer; manual locking was insufficient to obtain shot noise limited sensitivity. Locking in the local oscillator arm was not critical over short time scales, and was performed manually.

6. Acknowledgments

This project was supported by a research grant from the Australian Research Council.
Malcolm Gray and Charles Harb are supported by Australian National University Graduate School Scholarships.

References:

1 P. Hello, "External Phase Modulation: upper limit for SNR", *VIRGO internal report*, Ref: 0.2.1.a, 1990.

2 C.N. Man, D. Shoemaker, M. Pham Tu , D. Dewey, "External modulation technique for sensitive interferometric detection of displacements", *Phys. Lett. A*,148, 8-16 (1990)

3 A.J. Stevenson, M.B. Gray, H-A. Bachor, D.E. McCelland, "Quantum noise limited interferometricphase phase measurements", *Applied Optics* Vol. 32, No 19, July 1990

4 B. J. Meers, K.A. Strain " Modulation, signal and quantum noise in interferometers", *Phys. Rev.* A 43, 5022-5029.

5 "Harmonic demodulation of non-stat shot noise", M.B. Gray, A.J. Stevenson, H-A. Bachor, D.E. McClelland, *Otpics Letters* Vol. 18, No 10.